Computational Methods for Analysis of Dynamic Events In Cell Migration

V. Castañeda[1,†], M. Cerda[1,†], F. Santibáñez[1], J. Jara[1,2], E. Pulgar[3], K. Palma[3], C.G. Lemus[3], M. Osorio-Reich[1], M.L. Concha[3], S. Härtel[1,*]

[1] *Laboratory for Scientific Image Analysis (SCIAN-Lab), Biomedical Neuroscience Institute BNI, Program of Anatomy and Development, ICBM, Faculty of Medicine, Universidad de Chile, Santiago, Chile.*

[2] *Department of Computer Sciences, FCFM, Universidad de Chile, Santiago, Chile.*

[3] *Laboratory of Experimental Ontogeny, Biomedical Neuroscience Institute BNI, Program of Anatomy and Development, ICBM, Faculty of Medicine, Universidad de Chile, Santiago, Chile.*

Abstract: Cell migration is a complex biological process that involves changes in shape and organization at the sub-cellular, cellular, and supra-cellular levels. Individual and collective cell migration can be assessed *in vitro* and *in vivo* starting from the flagellar driven movement of single sperm cells or bacteria, bacterial gliding and swarming, and amoeboid movement to the orchestrated movement of collective cell migration. One key technology to access migration phenomena is by using optical microscopy in combination with image processing algorithms. This approach resolves simple motion estimation (*e.g.* preferred direction of migrating cells or path characteristics), but can also reveal more complex descriptors (*e.g.* protrusions or cellular deformations). In order to ensure an accurate quantification, the phenomena under study, their complexity, and the required level of description need to be addressed by an adequate experimental setup and processing pipeline. Here, we review typical workflows for processing starting with image acquisition, restoration (noise and artifact removal, signal enhancement), registration, analysis (object detection, segmentation and characterization) and interpretation (high level understanding). Image processing approaches for quantitative description of cell migration in 2- and 3-dimensional image series, including registration, segmentation, shape and topology description, tracking and motion fields are presented. We discuss advantages, limitations and suitability for different approaches and levels of description.

Keywords: Cell migration, registration, segmentation, morphology, topology, tracking, motion estimation.

INTRODUCTION

Computational methods for analysis of dynamic events associated with cell migration have become increasingly important. The combination of light microscopy with digital image processing algorithms is a powerful tool to quantify dynamic events like cellular displacements, rearrangements and morphology changes at sub-cellular, cellular, and supra-cellular levels (Fig. **1**). Migratory events can be observed as individual and collective cell displacements, ranging from the flagellar driven movement of single sperm cells or bacteria [1], bacterial gliding and swarming [2], amoeboid movement [3], or the orchestrated movement of collective cell migration [4]. Depending on the context, different image processing algorithms have to be applied in order to quantify trajectories of single objects or to estimate the motion of organized cell groups or tissue. In addition, motion can be coupled with descriptors that characterize the shape or topology of single or grouped cells. In order to attain an accurate analysis of the biological phenomena under investigation, multiple factors need to be addressed. Experimental sample and acquisition settings such as field of view, sampling intervals (space and time), imaging technique, markers, fluorescence characteristics, quality of the microscopic signal, and camera/detector define the quality of the image series. In addition, images must be processed and analyzed with adequate mathematical and computational tools in order to access the desired information.

*Address correspondence to this author at the Laboratory for Scientific Image Analysis, ICBM, Facultad de Medicina, Universidad de Chile, Av. Independencia 1027, Independencia, Santiago, Chile; Tel/Fax: 56-2-29786366; Email: shartel@med.uchile.cl

† Both authors contributed equally to this review

A series of new microscopy techniques has emerged over the last years, which have increased the demand for advanced computational methods. For *in vivo* observations at sub-cellular levels, fluorescence microscopy has become a standard tool for 2D and 3D imaging. The use of various markers and filters also allow the observation of different structures, using a range of fluorescence channels simultaneously. Even though the spatial resolution of conventional optical microscopy is limited by Abbe's law of diffraction [5], resolution beyond the diffraction limit has been achieved with different approaches. Some methods like Structured Illumination Microscopy (SIM) [6, 7], Stimulated Emission Depletion (STED) [8], or 4π-microscopy [9], alter the shape and dimension of the basic emission unit of a molecular light source, the so-called Point Spread Function (PSF). Some techniques depend on extensive post processing of the acquired image series like Photo Activated Localization Microscopy (PALM) [10], Stochastic Optical Reconstruction Microscopy (STORM) [11], SIM, and Superresolution Optical Fluctuation Imaging (SOFI) [12, 13]. Readers interested in optics and image acquisition techniques and possible pitfalls are referred to specialized literature [14, 15, 16].

At cellular and supra-cellular levels, fast imaging techniques based on Spinning Disk Microscopy (SDM) [17] or Light Sheet Microscopy (LSM) [18, 19] can acquire images over a larger field of view more quickly and/or with greater depth, compared to conventional confocal laser scanning microscopes. In these novel techniques, basic image properties such as Signal-to-Noise Ratio (SNR), background characteristics, spatial and temporal sampling frequencies, and characteristic PSFs render very different raw materials for subsequent analysis. The choice of adequate methods for denoising, segmenting Regions Of Interest (ROIs), descriptors of shape and topology, tracking, and motion fields, requires a combination of backgrounds in mathematics, physics and computer science.

This review is intended to aid the life scientist deciding on whether to choose or adapt the most adequate computational strategy when it comes to the quantitative analysis of events associated with cell migration. The article organization is summarized in Fig. (**2**), which follows the typical pipeline of a computational image analysis of migration. In order to set a common language for the remaining sections, we define a digital image as an array of pixels in 2D (voxels in 3D), with numeric values (brightness in color channels) associated to each pixel that reflect optic properties of the sample. The numerical pixel values are determined by the bit depth of the image[1]. Commonly, digital images contain brightfield, phase contrast, or fluorescence readings corresponding to direct (autofluorescence) or indirect signals from a subjacent cellular structure (*e.g.* marked by fluorescent proteins, fluorescent antibodies, or quantum dots).

RESTORATION AND REGISTRATION

The quality of digital image series acquired by light microscopy is affected by multiple phenomena. The degree of photon noise and the shape of the microscopic PSF are a consequence of the optical components and the sensitivity of the sensors. In addition, sample drifts, rotations, or volumetric changes are either related to the mechanical stability of the system, such as platform movements in the *xyz* axis, or arise as a result of the evolution of the biological specimen during *in vivo* experiments. Finally, fast 3D scanning techniques may produce significant data volumes with empty or irrelevant information [20, 21]. This section discusses the related technical and experimental factors that need to be considered within an image processing framework to address image quality issues.

Restoration: denoising and deconvolution

The combination of high signal intensities from the desired microscopic structure, low signal intensities from the background of the image, and low pixel noise facilitates quantitative image processing [22, 23]. In order to maximize the success and robustness of posterior image processing routines, it is important to enhance the SNR [15], paying close attention to the image acquisition setup and the protocols prior the experiment such as labeling, mounting and configuration of the optical system during sample preparation.

While signals from non-desired structures (*e.g.* due to autofluorescence, spectral overlap, or unspecific labeling) can be minimized during sample preparation and acquisition, remaining fluctuations at the single pixel level, or so-called photon noise, affect virtually all acquired microscopic raw images. Only some superresolution techniques like PALM, STORM, SOFI, and its derivatives remove pixel noise as a result of their intrinsic

[1] The bit depth corresponds to the number of bits used to represent the intensity/color values, *e.g.* 8, 12, 16 bit codes per pixel allow 256, 4096, 65536 intensity values respectively.

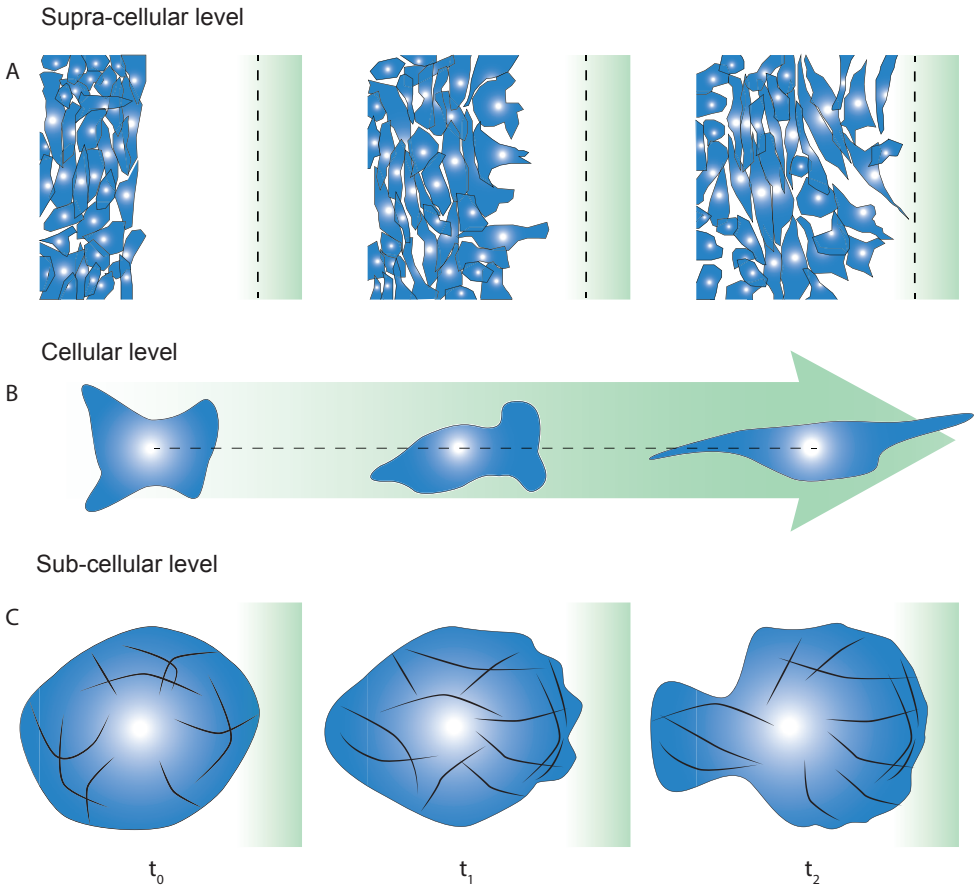

Fig. (1). Schema of cell migration at three levels: supra-cellular, cellular, and sub-cellular. (A) Epithelial cells tissue migrating during a wound healing assay. **(B)** Single cell migration. **(C)** Structural reorganization of internal actin fibers during cell migration. Cytoplasm (blue), nucleus (white), and directional migration signal (green).

localization and fluorescence emission profile [10, 12, 13].

For all other techniques, pixel-level noise and the 3D shape of the PSF are the major obstacles for correct signal detection [24]. This is especially true when weak excitation or fast imaging is required [25, 26]. In particular, for imaging near the diffraction limit of light microscopy, the size of the image pixels (or voxels in 3D) must become smaller than the size of the microscopic PSF (commonly determined by the Full Width at Half Maximum, FWHM). When the pixel-level noise becomes smaller than the sample signals which distribute as Gaussian PSFs over a vicinity of pixels, this spatial difference becomes a key element for efficient noise removal through deconvolution.

The so-called deconvolution process aims to reduce noise and simultaneously correct signal intensities using the shape of the microscopic PSF. Deconvolution is essential for a reliable quantification of fluorescent intensities of cellular structures or ion concentrations, especially near the resolution limit [24, 20]. Several deconvolution methods have been developed. Here we summarize classical, non-linear, and some more complex approaches.

Classical deconvolution algorithms [21] are based on linear approaches. For instance, the Wiener filter [27] was formulated for signal-independent additive Gaussian noise models providing a reduction of the effect of small coefficients in the Fourier domain. Another classical approach is the Tikhonov-Miller filter [28, 29], a linear filter which minimizes a functional which is the squared difference between the acquired image and a

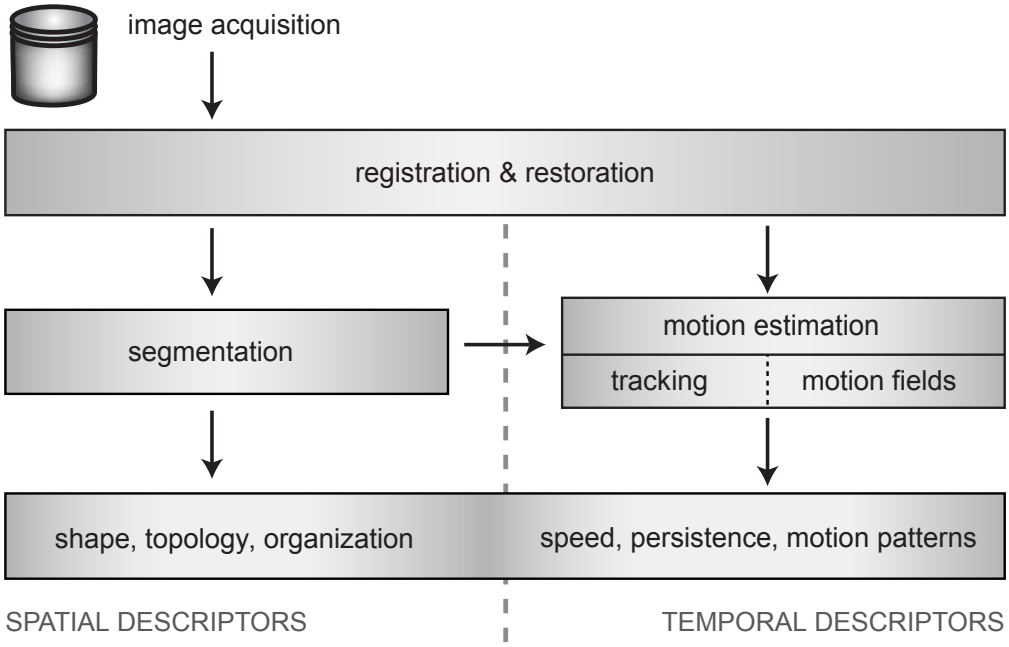

Fig. (2). Image processing pipeline for the analysis of cell migration.

blurred estimate of the original object regularized by a Tikhonov energy bound. The drawback of linear filters is that they cannot restrict the solution domain requiring the incorporation of additional constraints, *e.g.* finite support, smoothness, regularization terms, or non-negativity. The non-negativity constraint is a limitation since the intensities of the images represent light energy (number of photons) which cannot be negative [28].

Non-linear deconvolution approaches incorporate these constraints [21] through iteratively minimizing the error functions defined between the acquired image and blurred estimate of the original object [30]. Some examples of these approaches are Jansson-van Cittert method [21, 31], the Classical Maximum Likelihood Estimator (CMLE) [32], or the least-squares PSF fitting based on realistic 3D PDF models [33]. A common drawback for these algorithms is the demanding computational and time requirements of the iterative formulations.

Alternative deconvolution filtering techniques were recently proposed based on Wavelets [34, 35], sparse representations [25, 26] or space-variant blur approximations [36] in order to provide faster implementations over the iterative approaches.

Deconvolution software exist as custom built prototypes, open source projects (*e.g.* imageJ [37] and its extension FIJI [38]), optional commercial software features from microscope vendors, or packages from software providers. Deconvolution software should offer complete control to set or import parameters used during the microscopic acquisition, and be designed for easy incorporation into the daily routine of microscopic imaging [39, 40]. Some software packages offer batch processing to ease the user of manually setting physical parameters for deconvolution in each stack (*e.g.* Huygens Scripting Software from SVI [41]). Batch processing is an important feature for large data sets obtained from *in vivo* observations, especially in long term 3D experiments that can easily pile up terabytes of imaging data [17, 42]. Alternative providers like Zeiss [43] or AutoQuant [44] do not reveal the underlying principles of their physical, numerical, or probabilistic approaches, while others like SVI follow conventional theory.

Apart from following guidelines published in studies that compare the performance of different commercial and open source deconvolution packages (HuygensPro, AutoDeblur, Deconvolution Lab, Parallel Iterative Deconvolution and Iterative Deconvolve 3D) on synthetic and microscopic images [39, 40], we suggest direct testing of software demos with typical sample images of cellular

organelles like membranes, mitochondria and endoplasmic reticulum or fluorescent beads below the diffraction limit. An adequate deconvolution removes pixel noise and maintains signals from sub-cellular structures or point sources as Gaussian-like profiles reflecting the microscopic PSF without blurring. Figs. (**3A**,**3B**) shows microscopic spinning disk images before and after deconvolution on a supra-cellular level. Pixel noise, ill-defined membrane structures and blebs impede a clear definition of the cellular structures in Fig. (**3A**). Fig. (**3B**) is virtually free of pixel noise and structural details are outlined within the signals of the membrane bound fluorescent protein. The deconvolution process was carried out with Huygens Professional deconvolution software [41].

Registration

For a precise characterization of the growth and migration of cellular structures, spatial and temporal data alignment is essential [45]. In this context, image registration aims to estimate an optimal transformation between two images or volumes in order to minimize spatial and temporal misalignment.

Misalignment can stem from perturbations of the acquisition system, protocols, movement or the evolution of the specimens (*e.g.* restricted growth in sealed environments using agarose [46], or large migrations that require repositioning the sample) as well as from mathematical processing tools used in denoising (*e.g.* median filters with even kernel size). Formally, misalignment can be described as affine invariant transformations, a combination of translation, rotation, scaling, and tilts [47]. It is essential to remove drift artifacts in order to obtain precise descriptions of growth or shape changes during migration.

Cell migration studies may require encapsulation protocols that can contribute to misalignment between images. For example, in several *in vivo* studies of zebrafish development (*e.g.* neural crest migration) specimens must be embedded in agarose to track migration over long periods of times [48, 46]. During embryo development, translations and scaling of the sample are observed due to the shift of the focal plane within the growing embryo. Growth alone can create drift, which can be accentuated by encapsulation resulting in more complex deformations such as twists. Deformations need to be differentiated from cellular changes through 3D analysis and using prior knowledge of the cells from 2D images [49].

In general, there are two types of registration methods: (i) intrinsic methods which try to use the information present in the acquired images in order to find the best transformation for alignment, and (ii) extrinsic methods which use external references that can be tracked independently of intrinsic deformations [45].

Intrinsic and extrinsic registration methods first need to define a similarity metric between reference and target images, later they optimize a transformation that maximizes the chosen similarity coefficient [50]. Markelj *et al.* [51] presented similarity coefficients classification involving: (i) intensity-based analysis (*e.g.* sum of squared differences, normalized cross-correlation coefficients, or mutual information) that require normalized intensities or the calculation of a joint histogram [49], (ii) feature-based analysis (estimation of distances between corresponding points or feature metrics) as curvature-based registration [52], and (iii) optimization methods such as gradient descent [53], conjugate gradient descent, multiresolution search, or deterministic annealing.

Classical registration methods applied either to intrinsic or extrinsic registration consider drift and movement in the *xyz* axis through the alignment of the centers of gravity in combination with Median, Gaussian, or Kuwahara filters [54] (available as z-correction in an extra-tool for Huygens Deconvolution Software or ImageJ-FIJI). Rotational sample alignment approached by *rotation invariant moments of morphology* in combination with rotational axis based on Eigenvectors and Eigenvalues have been described in [55, 56, 57]. After translational and rotational alignment, image borders or irrelevant image sections can be removed by digital cutting.

Other algorithms have been proposed for registration to address more complex conditions of cell migration. In this context, we can find curve methods that provide a robust registration of images based on feature curve extraction modeled by a set of curves such as B-splines [58]. In addition, surface methods consider the boundaries or surfaces as similarity metrics by characterizing high contrast areas as references among images. Furthermore, Morphological Moments and Principal Axis establish reference elements of reduced dimensionality among images. This can simplify the description of the analysis of global similarities. More advanced approaches consider methods based on correlation and mutual information [49], Wavelets [35], or Soft Computing [45].

In general, registration processes balance the tradeoff between minimizing misalignment and conserv-

ing the actual translational, rotational, and volumetric changes that occur during cell migration. When feasible, the addition of external references helps simplify and optimize the registration process. Some of the algorithms used to address image registration are available in commercial [41] or open source software packages [37]. However, validation processes, particularly for non-rigid algorithms, still pose major challenges [50, 59].

SEGMENTATION

Segmentation is the process of identifying ROIs with a certain meaning from the rest of an image. Segmentation of ROIs is needed for the calculation of spatial and some temporal descriptors, including shape, topology, and organization (see "Shape and Topology") as well as motion related descriptors (see "Motion Estimation"). Simple criteria like grouping pixels by similarity (*e.g.* pixel intensity, texture), finding discontinuity regions (boundaries), or looking for known shapes or patterns can give a fast but rough estimation of the total number, size and spatial distribution of fluorescent structures like nuclei, vesicles or fibers since these structures have relatively homogeneous labeling. Images with poor signal quality issues (see "Restoration: denoising and deconvolution") and/or complex structures like membranes and their protrusions (*e.g.* blebs, filopodia) require more advanced techniques to detect subtle morphology features and patterns among variable image conditions. The combination of increasingly large data volume from acquisition techniques, together with the variability of cell and tissue characteristics within complex scenarios (*e.g.* densely packed cell arrangements or overlaps that impede even visual assessment) makes reliable and automated segmentation of migrating cells a constant challenge for improved computational methods [60].

Filtering and thresholding

Threshold segmentation is based on the selection of global or local intensity values (thresholds) that separate pixels in ROIs from the background. Thresholds can be constant or adaptive as function of global or local intensity features. They can be applied directly after registration and deconvolution, after applying additional filters for image smoothing or contrast enhancement, or by enhancing shape, texture, or boundaries. Filters are commonly implemented as discrete convolutions [56], where the choice of kernel size and values determine the enhancement. Popular filters like Canny and Sobel target ROI edges [61, 62] but, as is the case with many boundary detectors, they are prone to local irregularities or residual image noise. Following the filtering enhancement and thresholding strategy, Rapoport *et al.* [63] first filtered image artifacts with a quadratic optimization function with sparseness and smoothness regularizations, followed by a simple threshold to define the ROIs. In general, the selection of filters is completely dependent on the structure of the target ROIs, and strategic choices and adjustments lead to an improved segmentation. For example, the majority of nuclei can be segmented by direct intensity thresholds; however, a strategic filter choice (*e.g.* Laplace or oval shape filters) can enhance the contrast of the nuclei in relation to the background, prior to the threshold application, improving the final segmentation. To avoid manual thresholding, automatic threshold selection has been proposed [64], in order to maximize the intensity variance among two groups of pixels. More sophisticated threshold election based on clustering algorithms has also been proposed, and demonstrated superior performance over manual threshold selection [65].

Segmentation refinement

After thresholding, a rough approximation of the ROIs is obtained. Further refinements can be applied to connect, disconnect or improve ROI boundaries by taking into account morphology features such as boundary size, holes, orientation, and area. A popular method to separate ROIs is the watershed algorithm, which is used in many segmentation pipelines, as outlined by Khairy *et al.* [66]. The watershed algorithm interprets image intensities (or ROI distance maps) as topographic reliefs where intensity levels are analogues of altitude. Then, it simulates a rainfall that leads to water accumulations at topographic sinks. Finally, lakes are grown against the topographic gradients until they reach a saddle point or local maximum which separates the catchment area of a neighboring lake or region. These watersheds define borders that can be used to assign or separate fused ROIs. This method is fast, but can lead to oversegmentation when the image relief has too many local minima [66]. However, the number of local minima can be reduced by successively smoothing the image prior to applying the watershed. The smoothing approach results in a trade-off between too many ROIs and too many fused ROIs. For example, Harder *et al.* [67] segmented cells with a region adaptive threshold scheme, followed by an Euclidean distance transform applied to the ROIs

in the mask image, and then separated the joined regions based on the watershed algorithm.

Deformable model fitting

Deformable models define high-level ROI properties, typically related to morphology or image features. They allow final ROI representation improvement and segmentation of a wide range of shapes while at the same time dealing with issues like non-homogeneous ROI intensities or weak contrast. Deformable model segmentation methods are based on using Partial Differential Equations (PDEs) to solve mathematical optimization problems, stated as integral functions for minimization or maximization. Instead of explicitly defining an enhancement filter, these models define higher level ROI properties, such as size, boundary smoothness, image contrast or region homogeneity, which are weighted and balanced in a sum of terms over the input and the segmented image [68]. Strategies to solve these equations can be implemented with generic or *ad hoc* methods that can include application constraints such as interactivity or user clues, parameter flexibility, error tolerance, or computational performance. The optimization functions are commonly defined over the entire image, modeling ROI boundaries with parametric or implicit functions. Boundary models are suitable for finer representations by interpolation or refinement techniques, and thus are useful for obtaining more accurate estimations of ROI shape parameters.

Parametric models are often referred to as active contours or snakes [69, 70, 71, 72]. Implicit models are known as level-sets or geometric active contours, and have been reviewed in [73, 74]. Both models optimized energy functionals that included forces and restrictions to find contours with a minimum energy while staying close to image features (the most common are intensity changes). The PDEs are solved by iterative algorithms that start from an initial estimation of the ROIs. Common problems are initialization sensitivity (local optima), contour splitting or merging handling. In particular for fluorescence imaging, additional terms have to be introduced in the optimization functional to deal with boundaries in ROIs with missing information in 2D and 3D as in the subjective surfaces approach [75, 76]. To tackle sensitivity to initialization, Bergeest *et al.* [77] recently suggested a new term with convex energy functionals to find a global segmentation optimum in an efficient numerical calculation. Their approach does not suffer from local minima bias and the resulting segmentation is independent of the initialization. Zimmer *et al.* [78] included texture parameters into the snake model which led to cell segmentation in the presence of pseudopods; in addition, cell interactions were handled with repulsive contours. In [17, 79, 80], parametric 2D/3D active contour models have been applied to improve the segmentation of biological structures with satisfactory results, showing the versatility of the approach in general.

Other strategies

Other methods for segmentation include Hierarchical Self-Organizing Maps (HSOM) [81], supervised segmentation [82], and geodesic mean curvature flow [83]. Zheng *et al.* [81] proposed a hybrid segmentation that combined HSOM, histogram- and region-based techniques. Feature vectors of pixels are extracted in order to train the HSOM and to learn which groups have similar pixel properties used to later define preliminary regions. Final segmentation is obtained with region- and histogram-based techniques. Zaritsky *et al.* [82] presented a multi-cellular segmentation algorithm which learns how to classify basic image features of local patches within an image by using a support vector machine approach. Next, a refinement step, through a combination of classification and graph-cut segmentation is applied to optimize the ROIs and eliminate errors. Bourgine *et al.* [83] used a geodesic mean curvature flow model to filter noise from the input image. Finally, cell nuclei centers are detected and segmented with a generalized subjective surface method.

Extension to 3D

The advantage of working in 3D is the potential to avoid overlapping objects in 2D images. A major disadvantage is the increase in computation cost (memory and/or calculations) of the algorithms. In addition, the resolution of most confocal microscopy techniques in the xy-plane is at least three times better than in the z-axis [84]. Therefore, special adjustments need to be made such as image interpolation or anisotropic filtering. Segmentation can be directly performed at each xy-plane [85, 83] or extended to 3D. However, segmentation by processing each xy-plane requires further computations to connect the 2D ROIs along the z-axis (see Fig. **3**). The extension from 2D to 3D requires checking consistency for ROI connectivity, and optionally smoothness, in order to deal with the effect of the elongated voxel in the z-axis that distorts the surface properties

(see Fig. **3E**; the surface representation of the segmented parapineal cell after refinement with a 3D active surface model led to acceptable surface properties). Segmentation by extending to 3D also requires defining operations over voxels sets. For instance, Amat *et al.* [86] defined 3D ROIs by directly associating voxels into a super-voxel using a k-means approach, and obtained the final segmentation by identifying connected super-voxels.

Segmentation with temporal information

Melani *et al.* [85] applied a combination of subjective contours (level-sets) and optical flow [87] for motion estimation which handled smooth intensity changes in the image over time but was prone to the aperture problem [2]. Later, Mikula *et al.* [88] used a generalized subjective surface model [83] with a time-regularization constraint in the energy function. They assumed smooth contour displacements between consecutive time frames and performed a forward segmentation by incrementally linking the segmentation from previous frames. Then, the obtained trajectories were refined through 3D + time parametrized curves. They validated this approach with synthetic models and nuclei sequences with spherical shapes and smooth motion/deformations. Luengo-Oroz *et al.* [89] presented a method for 3D + time tracking and segmentation using convolution of 4D (3D + time) templates ("morphological elements") to represent and locate motion from nuclei and membranes. They segmented ROIs and their divisions through time by morphological operations such as erosion or dilation. They also presented a watershed algorithm extended to 3D including a viscous term to segment cell membranes, and performed tests with 2-photon and light sheet microscopy images. The algorithms performed poorly when segmenting membranes in noisy images, when portions of the image provide a weak signal, or when segmenting objects moving quickly.

SHAPE AND TOPOLOGY

Following segmentation, the next step for quantitative analysis of dynamic events in cell migration is selecting an adequate representation for the ROIs (*e.g.* the biological structures under study), and subsequent quantifications of shape, topology, and organization (Fig. **2**). Historically, biologists have used the term morphology to include both shape and topology descriptions [90], whereas in mathematics or computer science, morphology only refers to the characterization of the object shape. Topology, on the other hand, quantifies the existence of tunnels or holes within the object[3]. In this section, we review main descriptors for object shape and topology and their accuracy based on the selected strategy for object representation.

Object representation

A ROI can be seen as a set of image pixels or voxels resulting from image segmentation. One of the simplest ways to represent the segmented ROIs is to construct a "mask" image of the input, with pixels labeled with a common number for each ROI (background pixels labeled with zero). A special case is the *binary* mask, where no distinction between ROIs is made and there are only two pixel labels: one for the ROIs and zero for the background. ROIs can also be represented by subsets of boundary elements, ordered chain-codes [91], local features in spaces like Fourier descriptors [56], Gabor [92], wavelets [93], parametric curves or surfaces that encode the volume [94, 95], approximation of set volumes with geometrical primitives like parallelepipeds [96] or tetrahedra [97], or boundary regions with triangles [98]. In addition, higher level representations such as area, perimeter, Cartesian/Zernike [55, 56] moments, or even those derived from human cognition models [99] can be built. The choice of representation is closely related to the desired parameters to be extracted as discussed next, but it is also a trade-off between the precision of the representation and the computational load (memory and/or calculations) required for extracting information. Thus, high detail representations like voxel sets can be very accurate, but require a significant computational load.

Shape

Migration often involves variations of cell shape (see Fig. **1**). Some key migrational stages can be identified by studying the dynamics of cell deformation [100, 101, 102]. Also, the dynamics of local cell membrane deformations like blebs, filopodia, or lamellipodia can be associated to specific molecular mechanisms [103]. Thus,

[2] The motion of an object larger than the field of view is locally ambiguous. Thus, any local motion detector will respond identically to multiple types of motions for the object.

[3] In the sense of the geometric study of objects. In mathematics, the topology encompasses a broader range of properties for spaces related to connectedness.

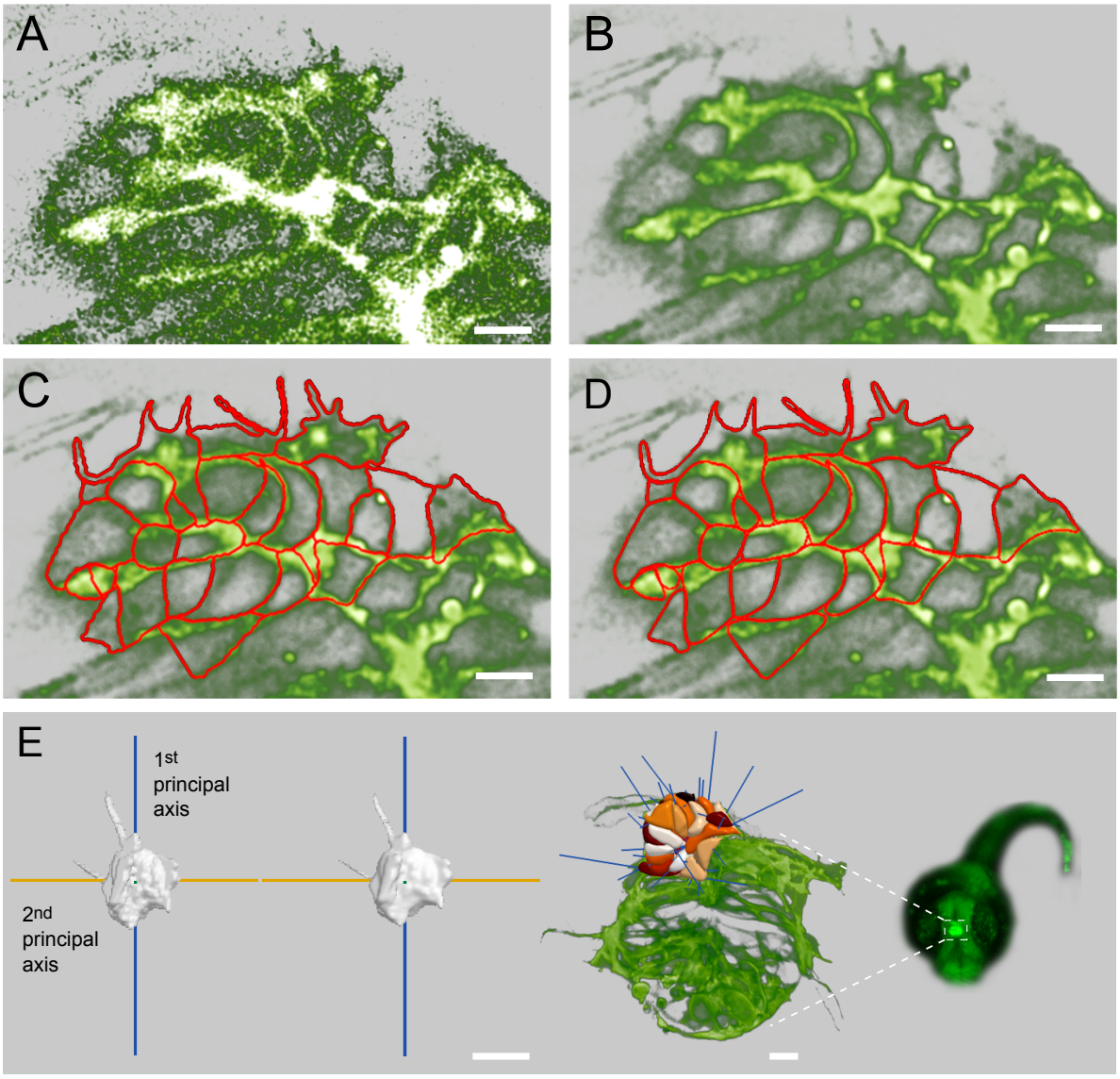

Fig. (3). Steps for 3D reconstruction of the parapineal nucleus in the brain of a zebrafish embryo. (A) Fluorescence SDM image (40×) of transgenic Tg(flh::EGFP) embryo at 38 hours post fertilization (hpf). **(B)** Cell membranes of the parapineal nucleus after deconvolution. **(C)** Cell membranes are manually outlined as red lines. (D) 2D active contour models drive polygons to (i) minimize perimeter through an elasticity parameter α, (ii) smooth the boundaries through a bending parameter β, (iii) maintain fine structures such as filopodia through a strong gradient vector field weighted by κ [72]. **(E)** Left: 2D active contours are used to form a preliminary 3D surface model of each cell. This surface model is a poor representation of the 3D morphology of the cell since it reflects the lower resolution along the z-axis using confocal microscopy. Right: 3D active surface models smooth the cell surface, especially along the z-axis, while maintaining fine structures and the bending in the xy-plane [79]. **(F)** Left: Active surface models of 24 parapineal cells with morphologic and organizational parameters during morphogenesis (*e.g.* 3D principal rotation axis are shown for each cell) [17]. Right: Orientation of the parapineal nucleus and brain within the zebrafish embryo. Scale bar 10 [μm].

global cell shape and local membrane events carry valuable information about cell migration.

Some commonly used shape descriptors for cells are: area (or surface area for 3D images), volume, center of mass, and bounding boxes [104, 105, 106, 102]. These descriptors can be understood as low order decompositions within the Cartesian moment theory [55]. However, higher order descriptions like kurtosis or skewness can also be computed analogous to statistical moments or mechanical moments of inertia. Moments are useful in calculating geometrical descriptors such as principal axes, through a combination of first and second order moments. Other approaches commonly used to compute shape in cell migration are descriptors such as the spindle factor [107] (relation between the minor and major axis as a measure of elongation), roundness [105, 108] (explained in detail by [109]), contour descriptors like perimeter [105] or convexity [110], and manual protrusion counting [111]. All of them rely strongly on the basic descriptors that can be extracted from Cartesian moments in combination with the convex hull [112], as well as contour measurements like perimeter [113] and curvature [56].

The computational precision of ROI descriptors such as area, principal axes, convex hull, perimeter, and roundness is closely related to the ROI representation [114]. For instance, calculating a perimeter measurement by counting edge pixels in a mask image has a 30% mean error using a 45 degree rotated square of size 100 pixels per side, but using a polygonal representation, the error can be reduced to 5%. The same exercise can be performed with the estimation of area in 2D, where pixel representation, for the same figure has less than 5% error. In general, the discrete nature (pixels or voxels) of computer images makes it necessary to implement boundary descriptions like polynomials or splines in order to access contour descriptors like perimeter, surface area, convex hull or curvature, with a certain degree of accuracy. However, description of complete regions like area, volume, or moments of morphology can be accurately estimated in pixel or voxel representation.

Topology

Topological descriptors are rarely mentioned as such, but they have been frequently used in biology and become increasingly important to characterize circuits or tubular networks. For instance, development studies describe cell spatial distribution in processes like epiboly [115] and formation of brain asymmetries in zebrafish [116]. Another example is the reorganization of actin fibers during cell migration illustrating structural change not captured using global shape descriptions. In actin fiber studies, descriptors like the number of fibers, intersections, and relative orientations, have been proposed as topological-like descriptors [117]. Also, dendritic development studies [118] have extracted descriptors such as the number and degree of branching, the number and length of segments, the growing angle (shown in Fig. **4A**), and have even classified neurons based on their structure [119].

A number of studies involving multi-cellular systems like tissues or organs, as well as their temporal evolution, require analysis of the spatial distribution of cells. For instance, relative distances among cell nuclei describe the compactness of the group [121], and relative orientation of the main axis reveals information about cell alignment [17]. In actin fiber-related studies, there are two main approaches to quantify fiber topology. The first approach describes fiber structures with global numbers such as the mean fiber orientation [120] (see Fig. **4B**) or mean fiber thickness [122]. The second approach identifies each individual fiber [117], by reducing a set of fibers into a 1D graph structure (line segments in a 2D or 3D space) known as a skeleton (Fig. **4A**). In neuronal development and migration studies, the most common approach to describe topology is to manually draw the structure, with the help of specialized software/hardware such as Neurolucida [123]. It is a complex and time consuming task that delivers good results by allowing the experienced biologist to directly identify the structure [124]. Interestingly, recent approaches from computer vision have emerged, mainly through the (semi) automatic reduction of structures into skeletons. These techniques have been applied in biological works (for a review see [125]), and semi-automatic implementation routines are readily available in software programs like ImageJ [37], Imaris [126], or Neuromorph [127]. Among these works, the direct skeletonization by morphological erosion of segmented ROIs is frequently reported [128, 129, 130, 131]. However, all of these approaches require some degree of manual intervention, or extremely carefully selection of input information [130], due to microscopy resolution constraints and segmentation errors.

Among the available methods to compute skeletons in the computer vision and geometry communities, we mainly found approaches based on two object represen-

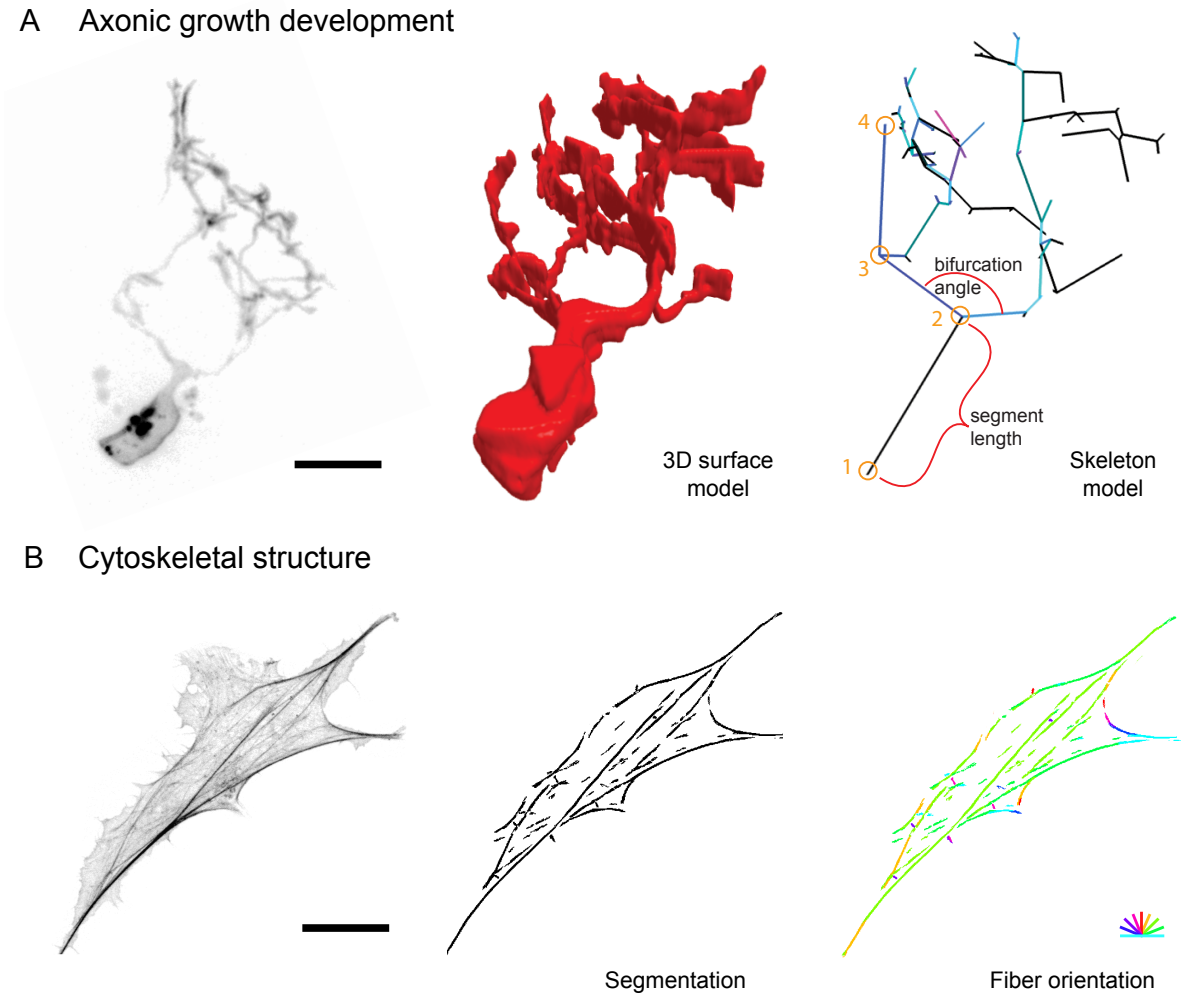

Fig. (4). Models and descriptors for structure analysis at different levels of organization. (A) Cellular level. Left: Raw maximum intensity image projection of an electroporated neuron with m-Cherry from the parapineal nucleus of zebrafish brain at 48 [hpf], using SDM (63×, z-step is 0.5 [μm], scale bar 9 [μm]). Middle: Surface model after manual segmentation of the neuron. Right: Skeleton representation of the neuron (left) and example descriptors such as node depth counted from the soma (orange circles). **(B)** Sub-cellular level. Left: Raw maximum intensity image projection from DITNC1 astrocytes transfected with actin-EGFP plasmid, using confocal microscopy (60×2.4, 7 z-steps of 1 [μm], scale bar 20 [μm]). Middle: Automatic segmentation was obtained by using a Gabor filter bank, similar to [120], and manual thresholding to highlight the actin filaments. Right: The segmented image was color-coded using the pixel-level orientation given by the Gabor filter bank max value.

tations: point clouds and surfaces. Point cloud based methods [132] are among the most widely used due to their simple implementation and speed (ROI pixels from mask images can be treated as point clouds in 2D and 3D). They are very sensitive to noise which leads to the generation of spurious branches. These methods are accurate for estimating global descriptors such as total structure length. However, they are not well suited for estimating edge or node number due to their noisy results and systematic underestimation of final segment length. Surface-based approaches for 3D objects [133, 129] are much less known in biology but have emerged as an alternative to stabilize topological descriptors measurements. They transform the object into a 1D representation by searching for the smallest representation (minimizing branches) which best represents the object structure, reducing the appearance of spurious objects. These methods achieve good estimates for almost all descriptors, but are more difficult to implement and apply due to their multiple configurable parameters. Surface-based methods offer promising new applications, beyond semi-automatic methods toward fully automatic topological quantification. Other authors have proposed elaborated pruning methods by measuring the importance of each point in the skeleton. For example, Reniers *et al.*'s method [134] can be incorporated into point cloud algorithms to control spurious branches by adding a new control parameter, the importance threshold.

MOTION ESTIMATION

So far, shape and topology descriptors can be used to address quantification of fixed as well as time-lapse images. In cell migration, in addition to discerning conformational changes, motion analysis is a key issue for understanding migrational processes. Migration can be seen in embryonic development, wound healing, and disease development such as tumor progression and tissue degradation, among others. Motion phenomena can be addressed for a single cell (see example in Figs. **1**,**5A**,**5B**) or groups of cells (Figs. **1**,**3**). One illustrative example is the study of embryogenesis in zebrafish, which requires tracking of individual cell nuclei and handling of cell division [66]. We distinguish between two main approaches for motion estimation: tracking and motion fields. The first requires ROI segmentation and aims to estimate individual trajectories, while the second aims to get a general estimation of motion patterns upon intensity changes over time, without depending on segmentation.

Tracking

In general, the process of identifying and linking segmented objects between frames in a given image sequence is called object tracking (sometimes "segmented object association"), with the linked trajectories giving the path of the object. Events like object collisions, appearances and disappearances can occur, and have to be handled by the algorithms in order to obtain correct trajectories.

Trajectories can be used to extract straight-forward descriptors such as estimated object velocities, as well as more complex measurements. We present common cell tracking algorithms and trajectory descriptors.

Tracking by detection basically consists of two stages: cell segmentation followed by association. First, object segmentation is performed for all time frames. Next, the objects must be linked in time, in order to obtain the complete path, which gives their trajectory. Tracking descriptors characterize each trajectory, representing for instance the faith map of individual cells. The linking of segmented objects frame-to-frame can be made by feature vectors, including spatial distance and similarity measures. Common features include mean cell intensity level and shape descriptors. For example, Harder *et al.* [67] used a feature vector of mean cell intensity, area, and center of mass. Next, they established a one-to-one correspondence by associating the closest cells, evaluating their similarity using the Euclidean distance between the corresponding feature vectors. An extended review can be found in Khairy *et al.* [66]. Similarity measures such as the Euclidean distance, can be effective if the feature vector remains stable along the trajectory, *i.e.* the tracked cell has a defined shape and a good temporal resolution. The similarity measure has been also extended to trajectories, for instance, by inspecting the *trustworthiness* of the tracking results, as proposed by Rapoport *et al.* [63]. The trustworthiness is measured by the ratio between the intersection of adjacent cell masks and the area of the cell mask. By using the largest forward and backward cell overlap, they selected a unique successor cell. From a set of short trajectories with high trustworthiness, they deduced the final trajectory and lineage of the every cell by the consistency of movement. A similar approach was presented by Chowdhury *et al.* in [135], based on bipartite graph matching and properties of Gaussian

distributions. These types of methods are used primarily when tracking isolated objects where the acquisition speed is fast enough to capture the object motion resulting in some overlap between the same ROI in consecutive frames. Typically, this is the case when image acquisition is fast enough to ensure individual ROI displacements of less than their average diameter between two frames. Some examples include imaging nuclei in phase-contrast or moving sperm, where tracking performs well and is easy to implement.

Tracking by model methods use a model with prior knowledge about the motion or feature changes through the migration. This implies that assumptions have to be made about the expected motion. From these, objects are registered frame by frame, generating the association among frames and, finally, the trajectories. For example, in sperm tracking, the assumption of non-cell-division can be made, and therefore a simple spatial distance can be used to generate the object association. Tracking by model approaches assume either a distribution for the feature vector, physical constraints, or most likely deformations along cell trajectories [136]. Debeir *et al.* [137] used the mean-shift algorithm, assuming a feature distribution that incorporates possible variations in cell morphology and grey-scale patterns present during cell mitosis. Kachouie *et al.* [138] introduced a probabilistic model (Bayesian) to address the spatiotemporal cell segmentation-association problem. When model knowledge is not directly available, the general tracking approach is based on image registration by making assumptions about object features, such as color conservation or motion constraints, and then trying to find a suitable transformation (rigid or deformable) between cells at two different or consecutive frames. The registration of the objects gives a relation between cells at different times. One example is the work of Sacan *et al.* [139] who tracked cell boundaries and intracellular points using active contours and optical flow estimation. Hand *et al.* [140] published a detailed paper reviewing five methods based on image registration, and compared their accuracy and computation costs. Yang *et al.* [141] presented an intensity-based non-rigid registration approach, which was extended to register 3D + time image series of moving cell nuclei. A hybrid approach by Xie *et al.* [142] addressed *E. Coli* migration in phase contrast images with low-contrast boundaries that changed very quickly. They proposed dynamically weighted similarity criteria by assuming constant speed and motion coherence. Using a model approach is more sophisticated than simply tracking by detection, and can be applied to more complex scenarios, *e.g.* nuclei tracking in fluorescence image sequences without sufficient temporal resolution, or nuclei changing shape over time.

Event handling Event handling is a critical step in the tracking pipeline, providing information to prevent incorrect object associations. To this end, it is necessary to know the kind of events that can occur, their characteristic features, and which actions need to be taken within the tracking pipeline. Common events are objects suddenly appearing or disappearing from the field of view, and moving objects that can touch or fuse. Some important events are: mitosis or cell division, cell fusion, fission, or apoptosis. Several works have addressed these events in the tracking pipeline. Rapoport *et al.* [63] detected mitosis observing the Y-shape produced in the trajectory and its characteristic spatiotemporal pattern. Kanade *et al.* [143] detected mitosis based on intensity change and handled objects coming into or leaving the field of view. Harder *et al.* [67] detected mitosis using an extension of the likelihood measure based on size and mean intensity of mother and daughter cell nuclei. Huh *et al.* [144] found mitosis events by using a detector based on a probabilistic model, which identified a video patch containing a mitotic event, and then localized the birth event. Amat *et al.* [145] developed a classifier using 3D Haar-like elliptical features which distinguished cell division events with high detection accuracy over millions of cells from light sheet microscopy images. Dufour *et al.* [22] detected when cells divided, entered or left the observation volume based on the location and shape of detected cells. Finally, Xie *et al.* [142] handled events in the case of drastic cell appearance change, overlapping and occlusion.

Tracking descriptors After tracking, the obtained set of trajectories is quantitatively analyzed in order to calculate descriptors that characterize migration dynamics. Some features are: motility, velocity, diffusivity, and proliferation.

-*Motility* can be estimated from straightforward trajectory descriptors such as length, displacement (distance between start and end points), comparative reference (maximum length or maximum distance traveled) and straightness index [60]. More complex descriptors can be calculated like the chemotactic index and the McCutcheon index, introduced by Meijering *et al.* [146].

Also, directional descriptors can be extracted at each trajectory point or at full trajectory level (persistence indicator).

-*Velocity/speed* can be directly calculated from a given cell trajectory, including instantaneous, mean, or maximum values. The speed can be computed from the displacement between two frames divided by the timing of the sequence. For example, analysis over the instantaneous speeds can be elaborated to obtain an arrest coefficient corresponding to the fraction of time that the object is not moving. Mean straight speed and mean curvilinear speed can be derived from the trajectories representing its linearity and forward/backward progression. An example with other velocity descriptors is shown in Figs. (**5A**,**5B**). Grouped data analysis was created with speed histograms in order to obtain statistics of the migration dynamics [60].

-*Diffusivity* aims to characterize motion with the help of Mean Squared Displacement (MSD). This measure relates observed movement with underlying physical phenomena. For instance, a linear relation between MSD and time implies a random walk motion ("free diffusion"). Other modes of motion that can be identified using MSD information are constrained diffusion (molecular binding, confined motion, motion impeded by obstacles) and motion due to a flux [60].

-*Proliferation:* cell division detection facilitates proliferation analysis by incorporating division counting, speed, and cell lineage. One example is the work of Harder *et al.* [67], who analyzed the resulting cell lineage from tracking and mitosis detection in order to extract mean displacements, calculate average cell motility and detect rare events from the cell lineage trees. Bhanson *et al.* [147] quantitatively analyzed cell growth rates by area, using the change of cell number in small regions as a rough but useful proliferation estimation. The review of Khairy *et al.* [66] illustrated how only by identifying proliferation events with color images, complex supra-cellular events like peripheral cell division waves in zebrafish embryogenesis can be visualized.

Motion fields

Optical Flow (OF) techniques are well established methods in computer vision to calculate motion fields, and have been proposed for the characterization of cell dynamics in recent years. OF methods relax the assumption of a conserved quantity (*e.g.* distance, shape and topology) during displacement. They focus on variations of intensities at local levels (pixels or small regions) to account for motion without requiring object segmentation. So far, OF applications in biology have been limited, but recent works have illustrated the maturation of these techniques for the quantification of dynamics in difficult scenarios [151, 152, 86]. In this section, we review OF methods and descriptors that can be elaborated in the context of cell migration.

OF methods in cell migration have been applied at sub-cellular, cellular, and supra-cellular levels. At sub-cellular level, neurotransmitter trafficking [150], calcium waves speed [153], and Golgi apparatus migration have been measured [154]. These works characterized speed and orientation of clearly defined objects: $GABA_B$ receptor subunits, calcium waves, Golgi (or transient Golgi). OF applications at cellular level are more frequent. Examples are mean cell motion estimation [155], by averaging vector field of voxels representing the cell [156, 140, 152, 157], or direct motion estimation of a set of voxels [86] or super-voxel [158]. Fig. (**5B**) is an example of motion estimation at supra-cellular level where object segmentation and tracking are difficult to obtain. In similar scenarios, OF has been applied to assess motion of unlabeled cells of *Dictyostelium* [159], or chick development [160], to estimate wound healing speed [161] or tissue flow [159, 157]. Tissue level OF applications aim to identify global motion patterns (rotation, speed) or clusters of moving cell. Other OF variants directly include parameters associated to cell migration as attractant spatial gradients [162].

OF methods start from the "grey value constancy" assumption [163]: a given object and background provide constant light intensity between two consecutive frames. The OF algorithm searches for the best vector field that explains intensity variations at the pixel level. It is implemented as a minimization process resulting in a vector field indicating horizontal and vertical motion (see Fig. **5B**). One of the first methods to compute OF was proposed by Lucas & Kanade [164] as a least-squares minimization. Their method performed well in corners [165] but failed at straight edges due to the aperture problem [166]. Horn & Schunck [163] proposed an alternative minimization algorithm by introducing an additional smoothness constraint. The algorithm diffuses information from corners to straight-edge regions with the additional cost of removing discontinuities. A first review was presented by [167], and a general computer vision benchmark database was proposed by [168]. In a related approach by Bruhn *et al.* [149], anisotropic diffusion was introduced to carry information from corners

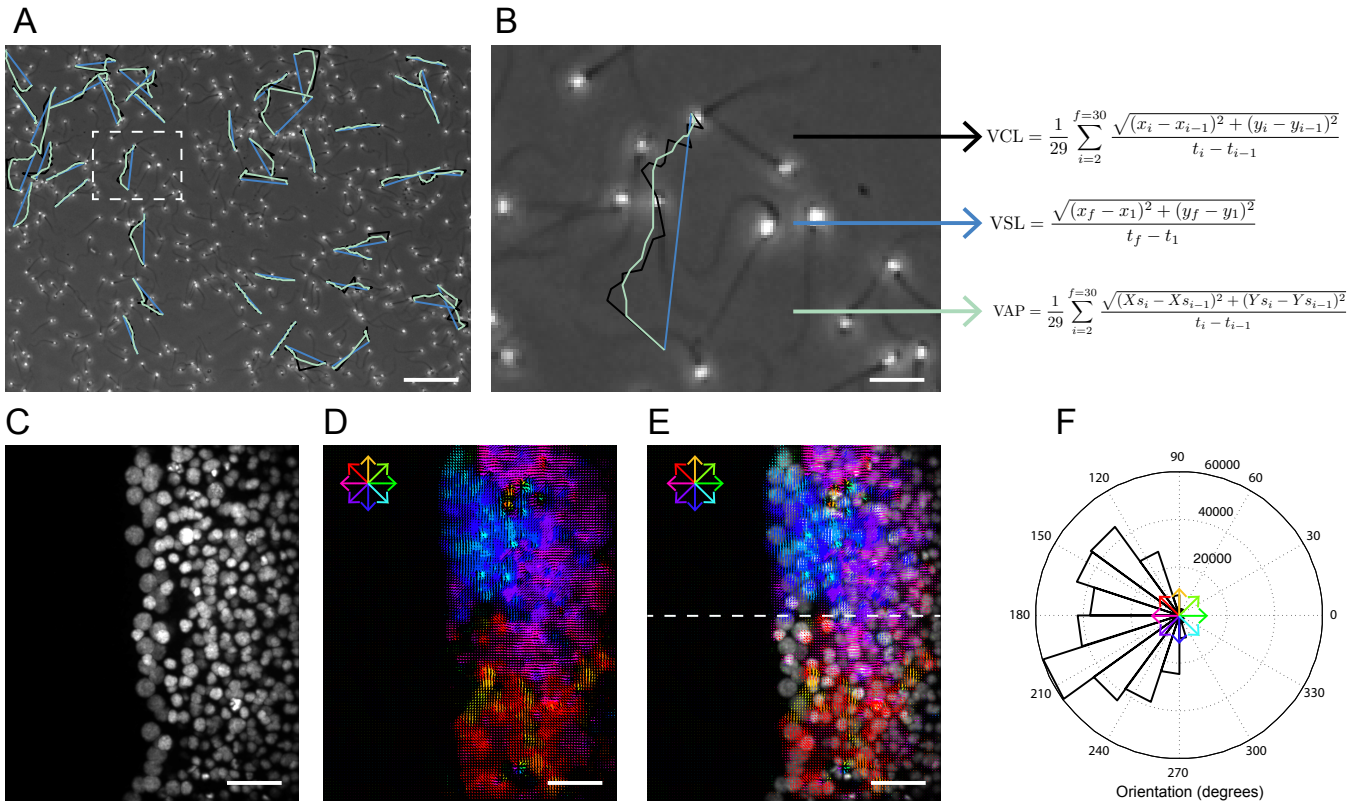

Fig. (5). Object tracking versus optical flow (OF) for motion estimation. **(A)** Human sperm motility analysis performed by tracking sperm trajectories for $1s$ at sampling rate of 30 frames per second (fps) with bright field microscopy. Scale bar 46 [μm]. The first image is shown together with paths that characterize different displacements of more than 67 [μm]. **(B)** Magnification of the white square in **(A)**. Scale bar 9 [μm]. The blue path shows the linear displacement between the starting point (x_1, y_1) and the end point (x_f, y_f); it is used to calculate the "velocity of the straight line" (VSL). The black path connects the position of the sperm head at each time and is used to calculate the "velocity of the curved line" (VCL). The green path connects the average positions (Xs, Ys) using a 5-frame sliding window, and defines the "velocity of the average path" (VAP). From VSL, VCL, and VAP, a series of additional path descriptors can be derived which characterize human or animal sperm motility for scientific or diagnostic purposes (see text and [148]). **(C-F)** OF motion estimation of enveloping layer, epiblast and yolk cell nuclei during zebrafish gastrulation. **(C)** z-Projection from fluorescence SDM images of cell nuclei expressing H2B-RFP mRNA at 5.3 [hpf], dorsal view (25$\times$, 0.005 [fps]), with vegetal pole to the left and animal pole to the right. **(D)** Color-coded OF vector field (one vector each 8 pixels) for two time steps, calculated by the combined local-global OF method [149, 150] (parameters: α =2, ρ =0). **(E)** Merged images from **(C)** and **(D)**. **(F)** The orientation histogram reveals one primary direction of migration to the vegetal pole with two sub-populations: one around 140 and one around 210 degrees, representing epiboly movement biased towards the embryo dorsal midline (dotted line) during early zebrafish gastrulation [115]. Scale bar 10 [μm].

to edges. Bruhn *et al.*'s approach preserved discontinuities in the OF field and extended the range of detectable motion through multi-scale analysis [169]. Despite the interesting perspective of these methods and their wide use in computer vision, very few applications have been described in cell migration or even in biology. Mainly the complex nature of the methods (minimization algorithms), and the multiple adjustable parameters have made the adoption of these methods difficult. Our group has recently started to systematically investigate the performance of different OF techniques for motion analysis of fluorescent point signals in microscopic image series [150]. So far, OF techniques without multiscale implementations can predict motions within an error of 3% for small displacements. However, the criteria for optimum parameter combinations for the calculation of the vector fields must be chosen carefully and depends on the temporal sampling frequencies. These methods pose an interesting perspective in quantifying cell migration [170] without explicit segmentation. For the interested researcher, we suggest some OF implementations available from the Image Processing On Line (IPOL) repository [171].

Descriptors from OF The output of any of the above mentioned OF methods is a vector field: the direction of the motion and its speed are available for each pixel. The most straightforward information that can be computed are mean speed and motion direction within ROIs [156, 140, 157, 86]. However, this operation requires object segmentation. Another approach is to search for simple motion patterns, for instance rotational patterns [160], or more complicated patterns like protrusion formation [155]. For a general pattern analysis, OF can be decomposed into translation, rotation, and convergence motions [172], an idea that has been applied to quantify wound healing dynamics in [161].

FINAL REMARKS

We have presented principles, features, main drawbacks, and advantages of presently applied image processing approaches for the analysis of dynamic events in cell migration. We discussed the main criteria in selecting the most suitable techniques for a given experimental setup. Additionally, we have introduced main preprocessing operations for denoising and registration, to allow biologists to correctly prepare their raw data for subsequent image processing methods like segmentation, shape & topology characterization or tracking. Altogether, we expect that our review of current and emerging methods in computer vision applied to cell migration studies stimulates future efforts within this field.

ACKNOWLEDGMENTS

Research in SCIAN-Lab (SH) is funded by the Chilean Fondo Nacional de Desarrollo Científico y Tecnológico FONDECYT grant No.1120579, the Fondo de Fomento al Desarrollo Científico y Tecnológico FONDEF D07I1019, the Chilean Millennium Science Initiative (ICM, P09-015-F), the Universidad de Chile U-Redes Project: BioMed-HPC and the Advanced Imaging & Bioinformatics Initiative AI·BI (www.aibi.cl). VC and MCe are funded by postdoctoral fellowships from ICM P09-015-F. VC is also funded by the U-Redes Project: BioMed-HPC and FONDEF D07I1019. MCe is also funded by FONDECYT grant No.1120579 and the Latin American Cancer Research Network (US-LACRN). FS, JJ, EP, CGL and KP are funded by CONICYT doctoral fellowships and supported by ICM P09-015-F. EP, KP, CGL and MCo are also funded by FONDECYT grant No.1120558 and ICM P09-015-F. The authors thank Dr. Areli Cárdenas from Prof. Lisette Leyton's Lab at BNI, for providing images and discussion of Fig. (**4B**).

REFERENCES

[1] Henrichsen J. Bacterial surface translocation: A survey and a classification. Bacteriol Rev 1972; 36(4): 478–503.
[2] Mignot T, Shaevitz J, Hartzell P, Zusman D. Evidence that focal adhesion complexes power bacterial gliding motility. Science 2007; 315(5813): 853–6.
[3] Allen R, Allen N. Cytoplasmic streaming in amoeboid movement. Annu Rev Biophys Bio 1978; 7: 469–95.
[4] Rorth P. Collective cell migration. Annu Rev Cell Dev Bi 2009; 25(1): 407–29.
[5] Abbe E. Beiträge zur Theorie des Mikroskops und der mikroskopischen Wahrnehmung. Arch f Mikroskop Anat 1873; 9: 413–20.
[6] Schermelleh L, Carlton P, Haase S, et al. . Subdiffraction multicolor imaging of the nuclear periphery with 3D structured illumination microscopy. Science 2008; 320: 1332–6.
[7] Gustafsson A. From quantum-well wires to nanowires as studied by cathodoluminescence imaging and spectroscopy. Scanning 2008; 30: 1–7.
[8] Hell S, Dyba M, Jakobs S. Concepts for nanoscale resolution in fluorescence microscopy. Curr Opin Neurobiol 2004; 14(5): 599–609.
[9] Hell S, Stelzer E, Lindek S, Cremer C. Confocal microscopy with an increased detection aperture: type-B 4π confocal microscopy. Opt Lett 1994; 19(3): 222–4.
[10] Betzig E, Patterson G, Sougrat R, et al. . Imaging intracellular fluorescent proteins at nanometer resolution. Science 2006; 313(5793): 1642–5.
[11] Rust M, Bates M, Zhuang X. Sub-diffraction-limit imaging by stochastic optical reconstruction microscopy (STORM). Nat Methods 2006; 3: 793–6.
[12] Dertinger T, Colyera R, Iyer G, Weiss S, Enderlein J. Fast, background-free, 3D super-resolution optical fluctuation imaging (SOFI). P Natl Acad Sci USA 2009; 106(52): 22287–92.

[13] Dertinger T, Colyer R, Vogel R, Enderlein J, Weiss S. Achieving increased resolution and more pixels with superresolution optical fluctuation imaging (SOFI). Opt Express 2010; 18(18): 18875–85.

[14] North A. Seeing is believing?. J Cell Biol 2006; 172(1): 9–18.

[15] Pearson H. The good, the bad and the ugly!. Nature 2007; 447: 138–40.

[16] Egner A, Schrader M, Hell S. Refractive index mismatch induced intensity and phase variations in fluorescence confocal, multiphoton and 4π-microscopy. Opt Commun 1998; 153: 211–7.

[17] Härtel S Jara J, Lemus C, Concha M. 3D Morpho-Topological Analysis of Asymmetric Neuronal Morphogenesis in Developing Zebrafish. Computational Modelling of Objects Represented in Images. Fundamentals, Methods and Applications. Ed. João Manuel Tavares & Jorge Nata, Taylor and Francis Group 2007: 215–20.

[18] Huisken J, Swoger J, Bene FD, Wittbrodt J, Stelzer EHK. Optical sectioning deep inside live embryos by selective plane illumination microscopy. Science 2004; 305(5686): 1007–9.

[19] Keller P, Schmidt A, Wittbrodt J, Stelzer E. Development by scanned light sheet microscopy reconstruction of Zebrafish early embryonic. Science 2008; 322: 1065–9.

[20] Biggs DS. *3D deconvolution microscopy*. John Wiley & Sons, Inc. 2001.

[21] Sarder P, Nehorai A. Deconvolution methods for 3-D fluorescence microscopy images. IEEE Signal Proc Mag 2006; 23(3): 32–45.

[22] Dufour A, Shinin V, Tajbakhsh S, Guillen-Aghion N, Olivo-Marin JC, Zimmer C. Segmenting and tracking fluorescent cells in dynamic 3-D microscopy with coupled active surfaces. IEEE Transactions on Image Processing 2005; 14(9): 1396–410.

[23] Biggs D. A Practical guide to deconvolution of fluorescence microscope imagery. Microscopy Today 2010; 18: 10–4.

[24] Fink C, Morgan F, Loew M. Intracellular Fluorescent Probe Concentrations by Confocal Microscopy. Biophys J 1998; 75: 1648–58.

[25] Dupe F, Fadili MJ, Starck J. In: Deconvolution of confocal microscopy images using proximal iteration and sparse representations, Proceedings of the *5th IEEE International Symposium on Biomedical Imaging (ISBI)* 2008; pp. 736–9.

[26] Carlavan M, Blanc-Feraud L. Sparse Poisson noisy image deblurring. IEEE T Image Process 2012; 21(4): 1834–46.

[27] Sekko E, Thomas G, Boukrouche A. A deconvolution technique using optimal Wiener filtering and regularization. Signal Processing 1999; 72(1): 23 - 32.

[28] van Kempen GMP. Image restoration in fluorescence microscopy. 1998.

[29] Ramani S, Vonesch C, Unser M. Deconvolution of 3D fluorescence micrographs with automatic risk minimization, Proceedings of the *Biomedical Imaging: From Nano to Macro, 2008. ISBI 2008. 5th IEEE International Symposium on* 2008; pp. 732-735.

[30] Soulez F, Denis L, Tourneur Y, Thiebaut E. In: Blind deconvolution of 3D data in wide field fluorescence microscopy, Proceedings of the *9th IEEE International Symposium on Biomedical Imaging (ISBI)* 2012; pp. 1735–8.

[31] Quammen CW, Feng D, Taylor II, Russell M. Performance of 3D Deconvolution Algorithms on Multi-Core and Many-Core Architectures Available at: `http://www.cs.unc.edu/techreports/09-001.pdf` [accessed April, 2013].

[32] Keuper M, Temerinac-Ott M, Padeken J, et al. . In: Blind deconvolution with PSF regularization for wide-field microscopy, Proceedings of the *9th IEEE International Symposium on Biomedical Imaging (ISBI)* 2012; pp. 1292–5.

[33] Kirshner H, Aguet F, Sage D, Unser M. 3-D PSF fitting for fluorescence microscopy: Implementation and localization application. J Microsc 2013; 249(1): 13–25.

[34] Vonesch C, Unser M. In: A fast thresholded Landweber algorithm for general wavelet bases: Application to 3D deconvolution microscopy, Proceedings of the *5th IEEE International Symposium on Biomedical Imaging (ISBI)* 2008; pp. 1351–4.

[35] Vonesch C, Unser M. A fast multilevel algorithm for Wavelet-regularized image restoration. IEEE T Image Process 2009; 18(3): 509–23.

[36] Ben Hadj S, Blanc-Feraud L. In: Modeling and removing depth variant blur in 3D fluorescence microscopy, Proceedings of the *IEEE International Conference on Acoustics, Speech and Signal Processing (ICASSP)* 2012; pp. 689–92.

[37] Schneider CA, Rasband WS, Eliceiri KW. NIH Image to ImageJ: 25 years of image analysis. Nature Methods 2012; 9(7): 671–5.

[38] Schindelin J, Arganda-Carreras I, Frise E, et al. . FIJI: an open-source platform for biological-image analysis. Nature methods 2012; 9(7): 676–82.

[39] Griffa A, Garin N, Sage D. Comparison of deconvolution software in 3D microscopy: A user point of view—part 1. G.I.T. Imaging & Microscopy 2010; 12(1): 43–5.

[40] Griffa A, Garin N, Sage D. Comparison of deconvolution software: A user point of view—part 2. G.I.T. Imaging & Microscopy 2010; 12(3): 41–3.

[41] Huygens Software by Scientific Volume Imaging, Scientific Volume Imaging B.V. (SVI). Available at: `http://www.svi.nl/HuygensSoftware` [accessed April, 2013].

[42] Ahrens M, Orger M, Robson D, Li J, Keller P. Whole-brain functional imaging at cellular resolution using light-sheet microscopy. Nat Methods 2013; 1: 43–5.

[43] AxioVision 4 Module 3D Deconvolution, Carl Zeiss Microscopy, LLC, United States. Available at: `https://www.micro-shop.zeiss.com/?l=en&p=us&f=e&i=10224&h=25&n=0&sd=000000-1235-922` [accessed April, 2013].

[44] AutoQuant X3, Bitplane AG. Available at: `http://www.bitplane.com/go/products/autodeblur` [accessed April, 2013].

[45] Wyawahare V, Patil PM, Abhyankar HK. Image Registration Techniques: An overview. International Journal of Signal Processing, Image Processing and Pattern Recognition 2009; 2(3): 11–28.

[46] Hardin J. Confocal and Multi-Photon Imaging of Living Embryos, *Handbook Of Biological Confocal Microscopy*; Pawley JB, Ed. Springer US 2006; pp. 746–68.

[47] Arganda-Carreras I, Sorzano C, Thévenaz P, et al. . Non-rigid consistent registration of 2D image sequences. Phys Med Biol 2010; 55(20): 6215–42.

[48] Graeden E, Sive H. Live Imaging of the Zebrafish Embryonic Brain by Confocal Microscopy. J. Vis. Exp. 2009; 26: e1217.

[49] Lu X, Zhang S, Su H, Chen Y. Mutual information-based multimodal image registration using a novel joint histogram estimation. Comput Med Imag Grap 2008; 32(3): 202–9.

[50] Hutton BF, Braun M. Software for image registration: Algorithms, accuracy, efficacy. Semin Nucl Med 2003; 33(3): 180–92.

[51] Markelj P, Tomazevic D, Likar B, Pernuo F. A review of 3D/2D registration methods for image-guided interventions. Med Image Anal 2012; 16(3): 642–61.

[52] Alyuz N, Gokberk B, Dibeklioglu H, Akarun L. In: Component-based registration with curvature descriptors for expression insensitive 3D face recognition, Proceedings of the *8th IEEE International Conference on Automatic Face Gesture Recognition (FG)* 2008; pp. 1–6.

[53] Klein S, Pluim JP, Staring M, Viergever MA. Adaptive stochastic gradient descent optimisation for image registration. Int J Comput Vision 2009; 81(3): 227–39.

[54] Kuwahara M, Hachimura K, Eiho S, Kinoshita M. Processing of RI-Angiocardiographic Images, *Digital Processing of Biomedical Images*; Preston K, Onoe M, Eds. Springer US 1976; pp. 187–202.

[55] Prokop RJ, Reeves AP. A survey of moment-based techniques for unoccluded object representation and recognition. Graph Model Im Proc 1992; 54(5): 438–60.

[56] Nixon M, Aguado AS. *Feature Extraction & Image Processing*, 2nd ed. Academic Press 2008.

[57] Sroubek F, Flusser J. Multichannel blind iterative image restoration. IEEE T Image Process 2003; 12(9): 1094–106.

[58] Lu X, Zhang S, Zha Y, Chen Y. In: Three-dimensional nonrigid registration and fusion for image-guided surgery navigation system, Proceedings of the *International Conference on Medical Image Analysis and Clinical Applications (MIACA)* 2010; pp. 135–8.

[59] Gibson E, Fenster A, Ward AD. In: Registration accuracy: How good is good enough? a statistical power calculation incorporating image registration uncertainty, Proceedings of the *15th international conference on Medical Image Computing and Computer-Assisted Intervention (MICCAI)* 2012; 2; pp. 643–50.

[60] Meijering E, Dzyubachyk O, Smal I. Methods for cell and particle tracking. Method Enzymol 2012; 504: 183–200.

[61] Canny J. A Computational Approach To Edge Detection. IEEE T Pattern Anal 1986; 8(6): 679–98.

[62] Sobel IE. *Camera models and machine perception*. PhD thesis. Univ Stanford, CA, USA 1970.

[63] Rapoport DH, Becker T, Mamlouk AM, Schicktanz S, Kruse C. A novel validation algorithm allows for automated cell tracking and the extraction of biologically meaningful parameters. PLoS One 2011; 6(11): e27315.

[64] Otsu N. A Threshold Selection Method from Gray-Level Histograms. IEEE T Syst Man Cyb 1979; 9(1): 62–6.

[65] Dima A, Elliott J, Filliben J, et al. . Comparison of segmentation algorithms for fluorescence microscopy images of cells. Cytometry A 2011; 79(7): 545–59.

[66] Khairy K, Keller PJ. Reconstructing embryonic development. Genesis 2011; 49(7): 488–513.

[67] Harder N, Batra R, Gogolin S, et al. . In: Large-Scale Tracking for Cell Migration and Proliferation Analysis and Experimental Optimization of High-Throughput Screens, Proceedings of the *6th International Workshop on Microscopic Image Analysis with Applications in Biology (MIAAB)* 2011.

[68] Aubert G, Kornprobst P. *Mathematical problems in image processing: partial differential equations and the calculus of variations*; 147. Springer Science, Business Media 2006.

[69] Kass M, Witkin A, Terzopoulos D. Snakes: Active contour models. Int J Comput Vis 1988; 1(4): 321–31.

[70] Xu C, Prince JL. Snakes, Shapes, and Gradient Vector Flow. IEEE T Image Process 1998; 7(3): 359–69.

[71] Gunn SF, Nixon MS. A robust snake implementation; a dual active contour. IEEE T Pattern Anal 1997; 19: 63–8.

[72] Fanani M, Härtel S, De Tullio L, et al. . The action of sphingomyelinase in lipid monolayers as revealed by microscopic image analysis. Biochim Biophys ACTA - Biomembranes 2010; 1798(7): 1309–23.

[73] Osher S, Fedkiw RP. *Level set methods and dynamic implicit surfaces*. Applied mathematical science, New York, N.Y.: Springer 2003.

[74] Osher S, Fedkiw RP. Level set methods: An overview and some recent results. J Comput Phys 2001; 169: 463–502.

[75] Sarti A, Malladi R, Sethian JA. Subjective surfaces: A method for completing missing boundaries. P Natl A Sci USA 2000; 97(12): 6258–63.

[76] Zanella C, Campana M, Rizzi B, et al. . Cells Segmentation From 3-D Confocal Images of Early Zebrafish Embryogenesis. IEEE T Image Process 2010; 19(3): 770–81.

[77] Bergeest JP, Rohr K. Efficient globally optimal segmentation of cells in fluorescence microscopy images using level sets and convex energy functionals. Med Image Anal 2012; 16(7): 1436–44.

[78] Zimmer C, Labruyere E, Meas-Yedid V, Guillen N, Olivo-Marin JC. Segmentation and tracking of migrating cells in videomicroscopy with parametric active contours: A tool for cell-based drug testing. IEEE T Med Imaging 2002; 21(10): 1212–21.

[79] Fidorra M, García A, Ipsen J, Härtel S, L B. Lipid domains in giant unilamellar vesicles and their correspondence with equilibrium thermodynamic phases: A quantitative fluorescence microscopy imaging approach. Biochim Biophys ACTA - Biomembranes 2009; 1788(10): 2142–9.

[80] Schlapp G, Scavone P, Zunino P, Härtel S. Development of 3D Architecture of Uropathogenic Proteus mirabilis Batch Culture Biofilms - A Quantitative Confocal Microscopy Approach -. J Microbiol Methods 2011; 87(2): 234–40.

[81] Zheng C, Ahmad K, Long A, Volkov Y, Davies A, Kelleher D. In: Hierarchical SOMs: Segmentation of Cell-Migration Images, Proceedings of the *4th international symposium on Neural Networks (ISSN): Part II–Advances in Neural Networks* 2007; pp. 938–46.

[82] Zaritsky A, Natan S, Horev J, et al. . Cell motility dynamics: a novel segmentation algorithm to quantify multi-cellular bright field microscopy images. PLoS One 2011; 6(11): e27593.

[83] Bourgine P, Cunderlík R, Drblíková-Stavsová O, et al. . 4D embryogenesis image analysis using PDE methods of image processing. Kybernetika 2010; 46(2): 226–59.

[84] Lakowicz JR. *Principles of Fluorescence Spectroscopy*, 3rd ed. New York: Springer 2006.

[85] Melani C, Peyrieras N, Mikula K, et al. . In: Cells tracking in a live zebrafish embryo, Proceedings of the *Eng Med Biol Soc Ann* 2007; pp. 1631–4.

[86] Amat F, Myers EW, Keller PJ. Fast and robust optical flow for time-lapse microscopy using super-voxels. Bioinformatics 2013; 29(3): 373–80.

[87] Horn BK, Schunk BG. Determining optical flow. Artificial Intelligence 1981; 17: 185–204.

[88] Mikula K, Peyriéeras N, Remešíková M, Smíšek M. In: 4D Numerical Schemes for Cell Image Segmentation and Tracking, *Finite Volumes for Complex Applications VI Problems & Perspectives*; Fořt J, Fürst J, Halama J, Herbin R, Hubert F, Eds. Springer Berlin Heidelberg 2011; pp. 693-701.

[89] Luengo-Oroz MA, Pastor-Escuredo D, Castro-Gonzalez C, et al. . 3D+t Morphological Processing: Applications to Embryogenesis Image Analysis. IEEE T Image Proc 2012; 21(8): 3518-30.

[90] Thompson D. *On Growth*, 1st ed. N.Y. 11501: Dover Publications 1942.

[91] Proffitt D, Rosen D. Metrication errors and coding efficiency of chain-encoding schemes for the representation of lines and edges. Comput Vision Graph 1979; 10(4): 318–32.

[92] Zhang B, Shan S, Chen X, Gao W. Histogram of Gabor Phase Patterns (HGPP): A Novel Object Representation Approach for Face Recognition. IEEE T Image Process 2007; 16(1): 57–68.

[93] Othmani M, Bellil W, Ben Amar C, Alimi A. A novel approach for high dimension 3D object representation using multi-mother wavelet network. Multimed Tools Appl 2012; 59: 7–24.

[94] Lin WC, Fu KS. A syntactic approach to 3-D object representation. IEEE T Pattern Anal 1984; 6(3): 351–64.

[95] Carr JC, Beatson RK, Cherrie JB, et al. . In: Reconstruction and representation of 3D objects with radial basis functions, Proceedings of the *28th Annual Conference on Computer graphics and Interactive Techniques (SIGGRAPH)* 2001; pp. 67–76.

[96] Kim Y, Aggarwal J. Rectangular parallelepiped coding: A volumetric representation of three-dimensional objects. IEEE T Robotic Autom 1986; 2(3): 127–34.

[97] Hitschfeld-Kahler N. Generation of 3D mixed element meshes using a flexible refinement approach. Eng Comput 2005; 21: 101–14.

[98] Campbell R, Flynn P. A Survey of Free-Form Object Representation and Recognition Techniques. Comput Vis Image Und 2001; 81(2): 166–210.

[99] Martin A. The Representation of Object Concepts in the Brain. Annu Rev Psychol 2007; 58(1): 25–45.

[100] Doherty GJ, McMahon HT. Mediation, modulation, and consequences of membrane-cytoskeleton interactions. Ann Rev Biophys 2008; 37(1): 65–95.

[101] Jiang X, Bruzewicz DA, Wong AP, Piel M, Whitesides GM. Directing cell migration with asymmetric micropatterns. P Natl A Sci USA 2005; 102(4): 975–8.

[102] Blanchard GB, Adams RJ. Measuring the multi-scale integration of mechanical forces during morphogenesis. Curr Opin in Genet Dev 2011; 21(5): 653–63.

[103] Farsad K, Camilli PD. Mechanisms of membrane deformation. Curr Opin Cell Biol 2003; 15(4): 372–81.

[104] Zamir E, Katz B, Aota S, Yamada K, Geiger B, Kam Z. Molecular diversity of cell-matrix adhesions. J Cell Sci 1999; 112(11): 1655–69.

[105] Dalby M, Riehle M, Johnstone H, Affrossman S, Curtis A. In vitro reaction of endothelial cells to polymer demixed nanotopography. Biomaterials 2002; 23(14): 2945–54.

[106] Kim DH, Han K, Gupta K, Kwon KW, Suh KY, Levchenko A. Mechanosensitivity of fibroblast cell shape and movement to anisotropic substratum topography gradients. Biomaterials 2009; 30(29): 5433–44.

[107] Tse JR, Engler AJ. Stiffness Gradients Mimicking In Vivo Tissue Variation Regulate Mesenchymal Stem Cell Fate. PLoS One 2011; 6(1): e15978.

[108] Sołtys Z, Ziaja M, Pawliński R, Setkowicz Z, Janeczko K. Morphology of reactive microglia in the injured cerebral cortex. Fractal analysis and complementary quantitative methods. J Neurosci Res 2001; 63(1): 90–7.

[109] Russ JC. *Image Processing Handbook*, 5th ed. Boca Ratón, FL, USA: CRC Press, Inc. 2007.

[110] Rhee DY, Zhao XQ, Francis RJB, Huang GY, Mably JD, Lo CW. Connexin 43 regulates epicardial cell polarity and migration in coronary vascular development. Development 2009; 136(18): 3185–93.

[111] Bailly M, Yan L, Whitesides GM, Condeelis JS, Segall JE. Regulation of protrusion shape and adhesion to the substratum during chemotactic responses of mammalian carcinoma cells. Exp Cell Res 1998; 241(2): 285–99.

[112] Berg Md, Cheong O, Kreveld Mv, Overmars M. *Computational Geometry: Algorithms and Applications*, 3rd ed. Santa Clara, CA, USA: Springer-Verlag TELOS 2008.

[113] Coeurjolly D, Klette R. A comparative evaluation of length estimators of digital curves. IEEE T Pattern Anal 2004; 26(2): 252–8.

[114] Yang L, Albregtsen F, Lønnestad T, Grøttum P. In: Methods To Estimate Areas And Perimeters Of Blob-Like Objects: A Comparison, Proceedings of the *Workshop on Machine Vision Applications (IAPR)* 1994; pp. 27227–33.

[115] Concha M, Adams R. Oriented cell divisions and cellular morphogenesis in the zebrafish gastrula and neurula: a time-lapse analysis. Development 1998; 125(6): 983–94.

[116] Signore IA, Guerrero N, Loosli F, et al. . Zebrafish and medaka: model organisms for a comparative developmental approach of brain asymmetry. Philos T Roy Soc B 2009; 364(1519): 991–1003.

[117] Lichtenstein N, Geiger B, Kam Z. Quantitative analysis of cytoskeletal organization by digital fluorescent microscopy. Cytometry A 2003; 54(1): 8–18.

[118] Uylings H, Pelt J. Measures for quantifying dendritic arborizations. Network 2002; 13(3): 397–414.

[119] van Pelt J, Schierwagen A. Morphological analysis and modeling of neuronal dendrites. Math Biosci 2004; 188: 147–55.

[120] Zemel A, Rehfeldt F, Brown AEX, Discher DE, Safran SA. Optimal matrix rigidity for stress fiber polarization in stem cells. Nat Phys 2010; 6(6): 468–73.

[121] Tassy O, Daian F, Hudson C, Bertrand V, Lemaire P. A Quantitative Approach to the Study of Cell Shapes and Interactions during Early Chordate Embryogenesis. Curr Biol 2006; 16(4): 345–58.

[122] Yoshigi M, Clark EB, Yost HJ. Quantification of stretch-induced cytoskeletal remodeling in vascular endothelial cells by image processing. Cytometry A 2003; 55(2): 109–18.

[123] Halavi M, Hamilton KA, Parekh R, Ascoli G. Digital reconstructions of neuronal morphology: Three decades of research trends. Front Neurosci 2012; 6(49): 1–11.

[124] Jaeger D. *Computational neuroscience: realistic modeling for experimentalists*. CRC Press 2000.

[125] Donohue DE, Ascoli GA. Automated reconstruction of neuronal morphology: An overview. Brain Res Rev 2011; 67: 94–102.

[126] 3D & 4D Image Analysis for Microscopy, Bitplane AG. Available at: `http://www.bitplane.com/` [accessed April, 2013].

[127] Oberlaender M. *Three-dimensional reengineering of neuronal microcircuits : The cortical column in silico*. PhD thesis. Univ Heidelberg 2009.

[128] Glicksman M, Koss M, Fradkov V, Rettenmayr M, Mani S. Quantification of crystal morphology. J Cryst Growth 1994; 137: 1–11.

[129] Janoos F, Mosaliganti K, Xu X, Machiraju R, Huang K, Wong STC. Robust 3D reconstruction and identification of dendritic spines from optical microscopy imaging. Med Image Anal 2009; 13(1): 167–79.

[130] Short K, Hodson M, Smyth I. Spatial mapping and quantification of developmental branching morphogenesis. Development 2012; 140: 471–8.

[131] Weaver CM, Hof PR, Wearne SL, Lindquist WB. Automated Algorithms for Multiscale Morphometry of Neuronal Dendrites. Neural Comput 2004; 16: 1353–83.

[132] Bucksch A, Lindenbergh RC, Menenti M. In: SkelTre - Fast Skeletonisation for Imperfect Point Cloud Data of Botanic Trees, Proceedings of the *Eurographics Workshop on 3D Object Retrieval* 2009; pp. 13–27.

[133] Au OKC, Tai CL, Chu HK, Cohen Or D, Lee TY. Skeleton extraction by mesh contraction. ACM T Graphic 2008; 27(3): 1–10.

[134] Dennie R, van Wijk Jarke, Alexandru T. Computing multiscale Curve and surface skeletons of genus 0 shapes using a global importance measure. IEEE Trans Vis Comput Graph 2009; 14(2): 355–68.

[135] Chowdhury AS, Chatterjee R, Ghosh M, Ray N. In: Cell Tracking in Video Microscopy Using Bipartite Graph Matching, Proceedings of the *20th International Conference on Pattern Recognition (ICPR)* 2010; pp. 2456–9.

[136] Li K, Chen M, Kanade T, Miller ED, Weiss LE, Campbell PG. Cell population tracking and lineage construction with spatiotemporal context. Med Image Anal 2008; 12(5): 546–66.

[137] Debeir O, Van Ham P, Kiss R, Decaestecker C. Tracking of migrating cells under phase-contrast video microscopy with combined mean-shift processes. IEEE T Med Imaging 2005; 24(6): 697–711.

[138] Kachouie NN, Fieguth P, Ramunas J, Jervis E. Probabilistic model-based cell tracking. Int J Biomed Imaging 2006; 2006: 1–10.

[139] Sacan A, Ferhatosmanoglu H, Coskun H. CellTrack: an open-source software for cell tracking and motility analysis. Bioinformatics 2008; 24(14): 1647–9.

[140] Hand A, Sun T, Barber D, Hose D, Macneil S. Automated tracking of migrating cells in phase-contrast video microscopy sequences using image registration. J Microsc 2009; 234(1): 62–79.

[141] Yang S, Köhler D, Teller K, et al. . Non-rigid registration of 3-d multichannel microscopy images of cell nuclei. IEEE Trans Image Process 2008; 17(4): 493–9.

[142] Xie J, Khan S, Shah M. Automatic Tracking of Escherichia Coli in Phase-Contrast Microscopy Video. IEEE T Bio-med Eng 2009; 56(2): 390–9.

[143] Kanade T, Yin Z, A R, et al. . In: Cell Image Analysis: Algorithms, System and Applications, Proceedings of the *IEEE Workshop on Applications of Computer Vision (WACV)* 2011; pp. 374–81.

[144] Huh S, Ker DFE, Bise R, Chen M, Kanade T. Automated Mitosis Detection of Stem Cell Populations in Phase-Contrast Microscopy Images. IEEE T Med Imaging 2011; 30(3): 586–96.

[145] Amat F, Keller P. In: 3D Haar-Like Elliptical Features for Object Classification in Microscopy, Proceedings of the *10th IEEE International Symposium on Biomedical Imaging (ISBI)* 2013; pp. 1182-5.

[146] Meijering E, Smal I, Olivo-Marin J. *Time-Lapse Imaging*. Elsevier Academic Press 2008.

[147] Bahnson A, Athanassiou C, Koebler D, et al. . Automated measurement of cell motility and proliferation. BMC Cell Biol 2005; 6(1): 19.

[148] Busso D, Onate-Alvarado M, Balboa E, et al. . Sperm from protein NPC2-deficient mice have defective cholesterol content and reduced in vitro fertilizing ability. Reprod Fert Develop, in press.

[149] Bruhn A, Weickert J, Schnörr C. Lucas/Kanade Meets Horn/Schunck: Combining Local and Global Optic Flow Methods. Int J Comput Vision 2005; 61(3): 211–231.

[150] Delpiano J, Jara J, Scheer J, Ramírez OA, Ruiz-del Solar J, Härtel S. Performance of optical flow techniques for motion analysis of fluorescent point signals in confocal microscopy. Mach Vision Appl 2012; 23: 675–89.

[151] Hubený J, Ulman V, Matula P. In: Estimating Large Local Motion in Live-Cell Imaging Using Variational Optical Flow, Proceedings of the *2nd International Conference On Computer Vision Theory And Applications (VISAPP)* 2007; pp. 542–8.

[152] Roberts T, McKenna S, Du CJ, Wuyts N, Valentine T, Bengough A. Estimating the motion of plant root cells from in vivo confocal laser scanning microscopy images. Mach Vision Appl 2010; 21: 921–39.

[153] Buibas M, Yu D, Nizar K, Silva G. Mapping the Spatiotemporal Dynamics of Calcium Signaling in Cellular Neural Networks Using Optical Flow. Ann Biomed Eng 2010; 38: 2520–31.

[154] Ben-Tekaya H, Miura K, Pepperkok R, Hauri HP. Live imaging of bidirectional traffic from the ERGIC. J Cell Sci 2005; 118(2): 357–67.

[155] Dubin-Thaler BJ, Hofman JM, Cai Y, et al. . Quantification of Cell Edge Velocities and Traction Forces Reveals Distinct Motility Modules during Cell Spreading. PLoS One 2008; 3(11): e3735.

[156] Breen E, Williams K. Optical flow analysis of the ventral cellular layer of the migrating Dictyostelium discoideum slug. Microbiology 1994; 140(5): 1241–52.

[157] Huang G, Kim J, Huang X, Zheng G, Tokuta A. A Statistical Framework for Estimation of Cell Migration Velocity. Journal WSCG 2012; 20(1): 29–36.

[158] Achanta R, Shaji A, Smith K, Lucchi A, Fua P, Süsstrunk S. SLIC Superpixels Compared to State-of-the-Art Superpixel Methods. IEEE T Pattern Anal 2012; 34(11): 2274–82.

[159] Siegert F, Weijer CJ, Nomura A, Hidetoshi M. A gradient method for the quantitative analysis of cell movement and tissue flow and its application to the analysis of multicellular Dictyostelium development. J Cell Sci 1994; 107: 97–104.

[160] Cui C, Yang X, Chuai M, Glazier JA, Weijer CJ. Analysis of tissue flow patterns during primitive streak formation in the chick embryo. Dev Biol 2005; 284(1): 37–47.

[161] Ronot X, Doisy A, Tracqui P. Quantitative study of dynamic behavior of cell monolayers during in vitro wound healing by optical flow analysis. Cytometry 2000; 41(1): 19–30.

[162] Farrell BE, Daniele RP, Lauffenburger DA. Quantitative relationships between single-cell and cell-population model parameters for chemosensory migration responses of alveolar macrophages to C5a. Cell Mot Cytoskel 1990; 16(4): 279–93.

[163] Horn BKP, Schunck BG. Determining optical flow. Artif Intell 1981; 17: 185–203.

[164] Lucas BD, Kanade T. In: An Iterative Image Registration Technique with an Application to Stereo Vision, Proceedings of the *7th International Joint Conference on Artificial Intelligence (IJCAI)* 1981; pp. 674–9.

[165] Márquez-Valle P, Gil D, Hernández-Sabaté A. In: Error analysis for lucas-kanade based schemes, Proceedings of the *9th international conference on Image Analysis and Recognition* 2012; pp. 184–91.

[166] Movshon A, Adelson E, Gizzi M, Newsome W. The analysis of moving visual patterns. Exp Brain Res 1986; 11: 117–52.

[167] Barron JL, Fleet DJ, Beauchemin SS, Burkitt TA. In: Performance Of Optical Flow Techniques, 1994; 92; pp. 236–42.

[168] Baker S, Scharstein D, Lewis JP, Roth S, Black MJ, Szeliski R. A Database and Evaluation Methodology for Optical Flow. Int J Comput Vision 2011; 92(1): 1–31.

[169] Adelson EH, Anderson CH, Bergen JR, Burt PJ, Ogden JM. 1984, Pyramid methods in image processing. RCA Engineer 1984; 29(6): 33–41.

[170] Cerda M, Jara J, Córdova A, et al. . Optical flow for temporal events quantification in celullar events. IEEE T Bio-med Eng 2013; In preparation.

[171] Image Processing On Line (IPOL). Available at: `http://www.ipol.im/` [accessed April, 2013].

[172] Gibson JJ. *The Perception of the Visual World*. Boston, MA: Greenwood Pub Group 1950.